Four modes of optical parametric operation for squeezed state generation

U.L. Andersen[1,2,a], B.C. Buchler[1], P.K. Lam[1], J.W. Wu[1], J.R. Gao[3], and H.-A. Bachor[1]

[1] Department of Physics, Faculty of Science, The Australian National University, ACT 0200, Australia
[2] Department of Physics, Technical University of Denmark, 2800 Kgs. Lyngby, Denmark
[3] Institute of Opto-Electronics, Shanxi University, Taiyuan, Shanxi 030006, P.R. China

Abstract. We report a versatile instrument, based on a monolithic optical parametric amplifier, which reliably generates four different types of squeezed light. We obtained vacuum squeezing, low power amplitude squeezing, phase squeezing and bright amplitude squeezing. We show a complete analysis of this light, including a full quantum state tomography. In addition we demonstrate the direct detection of the squeezed state statistics without the aid of a spectrum analyser. This technique makes the nonclassical properties directly visible and allows complete measurement of the statistical moments of the squeezed quadrature.

PACS. 42.50.Dv Nonclassical states of the electromagnetic field, including entangled photon states; quantum state engineering and measurements

1 Introduction

The most well-known non-classical state of light is the so-called squeezed state. It is special since its optical noise is redistributed such that it is less in one quadrature than the standard quantum noise limit while the fluctuations are correspondingly larger in the orthogonal quadrature. Squeezed light has been generated for many years [1]. Several metrology applications have been developed, including gravitational wave detection [2], polarisation and Mach-Zehnder interferometry [3,4], atomic spectroscopy [5] and laser Doppler anemometry [6]. During the last few years, squeezed state experiments have been dominated by quantum information applications such as quantum nondemolition measurements [7,8], quantum teleportation [9–11], quantum computing [12,13], dense coding [14,15] and quantum cryptography [16–18]. They all rely on encoding information in more than one quadrature and will either require squeezed light directly, or entangled light beams which can be generated by combining, on a beam splitter, two squeezed beams [9,19]. Finally, a new class of applications of squeezed states has been proposed [20] and experimentally realised [21], where the spatial properties of the beam of light is modified. This can be used to improve the resolution in the measurement of very small displacements of the laser beam with a split detector below the quantum noise limit.

[a] *Present address*: Institute of Optics, Information and Photonics, Max-Planck Research Group, University of Erlangen-Nuernberg, 91058 Erlangen, Germany.
e-mail: `andersen@kerr.physik.uni-erlangen.de`

All these applications rely on a stable, reliable, strong and flexible squeezing source. Triggered by those requirements, recent developments of squeezed light sources have been focused on technical issues, such as reliability of the electronic locking loops and hence the long-term stability of the system. In addition, a flexible source is required since some applications require squeezed light with no coherent excitation (vacuum squeezing), others prefer light with either a small (dim squeezing) or a large (bright squeezing) coherent excitation. Finally, some applications are considerably simplified if the bright squeezed light has reduced phase quadrature noise, instead of the more common amplitude quadrature noise suppression.

An optical parametric amplifier (OPA) or oscillator (OPO) has proven to be the most efficient source of quadrature squeezed light. In a nondegenerate mode, the source generates two spatially separable quantum correlated fields which can be used to create two-mode squeezing and strong Einstein-Poldolsky-Rosen entanglement [25,26]. However, in this paper we focus on the degenerate OPA, which has a long standing reputation as a generator of single-mode squeezed light. In 1965, Takahashi [24] proposed that an optical parametric amplifier (OPA) can be regarded as a serious and very interesting candidate for squeezed state generation. In 1986, Wu *et al.* [27] demonstrated a sub-threshold OPO experiment and achieved 3.5 dB of vacuum squeezing. Polzik *et al.* extended this experiment and generated frequency tunable squeezed light for spectroscopy [5]. These experiments were performed with a MgO:LiNbO$_3$ and a KNbO$_3$ crystal

inside ring cavities respectively. Using a MgO:LiNbO₃ crystal as a monolithic cavity design Breitenbach *et al.* [28] obtained 5.5 dB whilst Lam *et al.* [29] achieved 7 dB of vacuum squeezing. Bright amplitude squeezing was first generated by Schneider *et al.* [30] and further improved in reference [31] where an impressive 6 dB of squeezing was obtained over many hours of operation. Breitenbach *et al.* [32] used optical homodyne tomography to create the phase-space distribution such as the Wigner function of squeezed fields from an OPA.

The aim of this paper is two-fold: first, using a monolithic OPO/A, we demonstrate reliable squeezing in four different modes of operation; vacuum squeezing, low power or *dim* amplitude squeezing, high power or *bright* amplitude squeezing and phase squeezing. Secondly, the correlations contained in squeezed light are visualised by two-dimensional correlation plots. All correlations at one frequency, both those caused by classical or those by quantum effects, are observed. It provides a deeper insight in the properties of nonclassical fluctuations since it directly shows the time evolution of the quantum noise in a state and hereby the correlation and not just the variances as displayed by a spectrum analyser.

2 Theoretical model for the OPA and the detection

A detailed theoretical analysis of the OPO and OPA has been published by other authors [22]. Here we summarise this work to provide a background to the results we are presenting in the following sections. We use a type I degenerate OPO or OPA where a second order nonlinear medium, placed inside an optical cavity, couples two optical waves; a harmonic wave of frequency ν_p (the pump) and a sub-harmonic wave of frequency $\nu = \nu_p/2$ (the signal). In some cases our device will be operated as an amplifier and we consider the configuration where a seed beam is injected into the back port of the cavity. Only the subharmonic field will be resonating inside the cavity and the quantum Langevin equation of motion for this field can then in the Heisenberg picture be written as:

$$\frac{\mathrm{d}a(t)}{\mathrm{d}t} = -\gamma a(t) + 2\sqrt{\mu}a(t)^\dagger B_{\mathrm{in}}(t) - \mu a(t)^\dagger a(t)^2$$
$$+ \sqrt{2\gamma_b}A_{\mathrm{in}}(t) + \sqrt{2\gamma_l}F_{\mathrm{in}}^l(t) + \sqrt{2\gamma_c}F_{\mathrm{in}}^c(t). \quad (1)$$

Here $a(t)$ is the boson annihilation operator for the subharmonic field inside the cavity. $F_{\mathrm{in}}^l(t)$ and $F_{\mathrm{in}}^c(t)$ are auxiliary beam operators, with zero mean, governing all losses inside the cavity and loss due to the output coupling. Furthermore $A_{\mathrm{in}}(t)$ and $B_{\mathrm{in}}(t)$ represent the input annihilation operators for the subharmonic (seed) and the harmonic modes (pump), respectively. Those operators are assumed to be independent noise sources and obey the following stochastic correlations:

$$\langle F_{\mathrm{in}}(t)F_{\mathrm{in}}^\dagger(t')\rangle = \langle A_{\mathrm{in}}(t)A_{\mathrm{in}}^\dagger(t')\rangle = \langle B_{\mathrm{in}}(t)B_{\mathrm{in}}^\dagger(t')\rangle$$
$$= \delta(t - t'). \quad (2)$$

The decay rate for internal losses is γ_l and the damping associated with the coupling mirror and back mirror is γ_c and γ_b, respectively. The total damping is denoted $\gamma = \gamma_c + \gamma_l + \gamma_b$. The strength of the interaction is characterised by the nonlinear coupling parameter μ, which is assumed to be independent of frequency [34]. Coupling between the two beams is ensured by the second term in equation (1), which is then responsible for the parametric gain and hence the squeezed state generation. Two-photon absorption is described by the third order term and can also, in some cases, lead to squeezing. However, this term is negligible when the OPA works as an de-amplifier, but becomes important in the case of the inverse process of amplification. The cavity is assumed to be in exact resonance with the subharmonic field. Finally, equation (1) is complemented with the boundary condition $A_{\mathrm{out}}(t) = \sqrt{2\gamma_c}a(t) - A_{\mathrm{in}}(t)$ creating a propagating beam which is detected. The time varying operators $A_{\mathrm{out}}(t)$ and $A_{\mathrm{out}}^\dagger(t)$ contain all signal information including modulation signals, classical noise, quantum noise and squeezing.

After expansion of the operators into a steady state amplitude, α, and time dependent fluctuating components, $\delta A(t)$, so that $A(t) = \alpha + \delta A(t)$, we linearise the the equations by retaining only first order fluctuation terms. The frequency noise spectrum may then be found by taking the Fourier transform of the linearised equations, and evaluating the variance in the frequency domain. In particular one obtains the spectra for the amplitude quadrature, $\delta X_{\mathrm{out}}^+(\Omega) = \delta A_{\mathrm{out}}(\Omega) + \delta A_{\mathrm{out}}^\dagger(\Omega)$, and the phase quadrature, $\delta X_{\mathrm{out}}^-(\Omega) = -\mathrm{i}(\delta A_{\mathrm{out}}(\Omega) - \delta A_{\mathrm{out}}^\dagger(\Omega))$.

When the injected seed field is in-phase with the pump field, the phase quadrature is squeezed, and when the two fields are out of phase with respect to each other, the amplitude quadrature is squeezed, hereby creating two different types of squeezing. Furthermore, the power of the seed field determines three different types of squeezing; vacuum squeezing, dim amplitude squeezing or bright amplitude squeezing associated with a vacuum, dim or bright seed field, respectively.

Detection of the quadratures of the light field usually involves a homodyne arrangement where the weak beam that is to be determined is mixed with a strong local oscillator on a beamsplitter as shown in Figure 1. The two output beams from the beamsplitter, δX_1 and δX_2, are sent to two high efficiency photodetectors that create photocurrents with fluctuations that are proportional to those of the photon fluxes. The bandwidth of the detection at this stage is set by the bandwidth of the photodiodes and the amplifiers in the detectors. By taking the difference between the two photocurrents the fluctuation statistic generated is proportional to that of the original signal from the OPA. The particular quadrature that is measured is determined by the phase of the local oscillator relative to the squeezed beam. The spectral density of the quadrature, for example amplitude $V_{\mathrm{out}}^+(\Omega)$ or the phase $V_{\mathrm{out}}^-(\Omega)$, can then easily be recorded using an electronic spectrum analyzer.
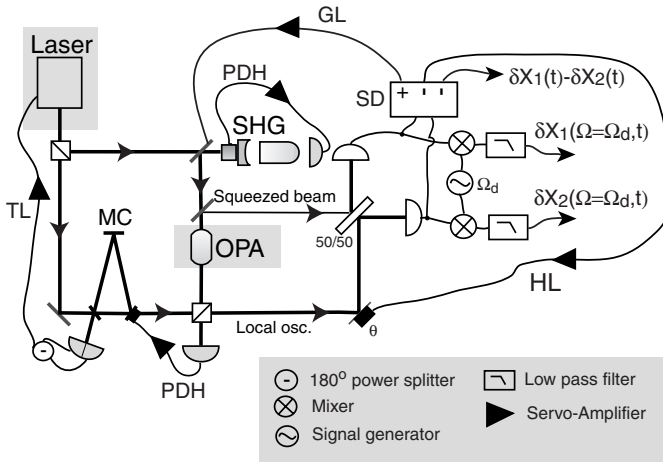
Fig. 1. Schematic of the experimental setup. SHG: second harmonic generator, OPA: optical parametric amplifier, MC: mode cleaner, 50/50: beamsplitter, which is 50% reflective, PDH: pound-Drever-Hall locking, TL: tilt-locking, GL: green phase locking, HL: homodyne phase locking, SD: sum and difference generator. Shown here are two ways of detecting the squeezing. The standard technique is to send the difference current $\delta X_1(t) - \delta X_2(t)$ to a spectrum analyser and record the power spectrum which is later normalised by the quantum noise. Alternatively one can measure the correlation between the individually mixed down output currents $\delta X_1(t)$ and $\delta X_2(t)$.

An alternative technique, that is presented in this paper, is to demodulate the individual detector photocurrents in the frequency interval $\Omega_d \pm \delta\Omega$ and to monitor them as an x/y plot on an oscilloscope. This technique records the joint density probability distribution of the noise for the two-mode squeezed state generated by the squeezed light beamsplitter.

3 Experimental details of the OPA system

Figure 1 shows a schematic diagram of our squeezed light source. The primary source in the experiment is a diode pumped Nd:YAG non-planar ring oscillator, which provides a frequency stable laser beam at 1064 nm. Most of the laser light is directed to a second harmonic generator, which serves as a pump for the OPA. This is a symmetric, 7.5 mm long, monolithic MgO:LiNbO$_3$ crystal with a 10 mm radius of curvature at the end faces. The back port of the OPA is highly reflective at both the harmonic and the subharmonic wavelengths whilst the coupler mirror is highly transmissive for the harmonic wave and 95.6% reflective at 1064 nm. The local oscillator and seed beam are passed through a mode-cleaning cavity. This improves the homodyne detection of the squeezing by ensuring a TEM$_{00}$ spatial mode. It also improves the squeezing bandwidth by filtering some of the technical noise from the seed beam. Depending on phase of the pump beam the injected seed beam is either subjected to amplification or de-amplification and finally sent to a homodyne measuring system.

Situations that call for squeezed light sources often require stable operation over many hours as long integration times are a crucial parameter in many applications. A technical goal during the construction of our squeezed light source was, therefore, to obtain a system that could generate stable squeezing for hours at a time. To reach this goal we employed numerous electronic feedback loops. Besides the temperature stabilisation required for the non-linear crystal ovens, we used five high-speed electronic servo control systems. The intrinsic frequency stability of the monolithic OPA cavity made it a good choice for the frequency reference. Thus the mode-cleaner was locked to the OPA cavity, the laser was locked to the mode-cleaner, while the SHG cavity was locked to the laser. The electronic feedback loops for locking the SHG cavity to the laser and the mode-cleaner to the OPA, were of the Pound-Drever-Hall (PDH) type [35]. Phase modulations at 30 MHz and 15 MHz were imposed onto the beams inside the SHG cavity and OPA cavity respectively. Error signals were then extracted using low noise photodiodes. In the case of the SHG, the transmitted field was monitored, while for the OPA, the reflected field was used to gather the locking signal. The photocurrent from the SHG detector was mixed down at 30 MHz to obtain an error signal that was processed by a servo controller and high-voltage amplifier before being fed-back to the piezo actuator in the SHG cavity. The signal reflected from the OPA cavity was mixed down at 15 MHz to obtain the error signal. This error signal was used to control the piezo actuator in the mode cleaner cavity and the temperature of the mode-cleaner spacer. The laser was locked to the mode cleaner via the tilt-locking method [36]. This is a modulation free technique that relies on spatial mode interference to gather the cavity locking signal. The method has proven to possess the same stability as the well-known PDH-method [37]. The tilt error signal was obtained on reflection from the mode-cleaner cavity and fed-back to the laser frequency.

The frequency locking servos described so far are enough to produce a squeezed beam, but not sufficient to guarantee stable squeezing detection. Also required is servo control of the squeezing phase. Locking to either amplitude or phase squeezing requires that the power of the beam transmitted through the OPA is maximised or minimised. This may be done using the 15 MHz modulation signal present on the squeezed beam. The power transmitted through the OPA cavity may be detected and the photocurrent mixed down to give an error signal. The disadvantage of this method is that it relies on down-stream detection of the squeezing. An alternative is to again look at signal reflected from the OPA cavity. The phase of the green beam was modulated at 30MHz due to the signal used for the SHG cavity locking. This has the effect of modulating the field reflected from the OPA at 30 MHz. The size and phase of this 30 MHz modulation depends on the phase between the pump and seed beams. Demodulation of the reflected power at 30 MHz therefore gives an error signal for green phase. Regardless of the method used, the green phase error signal was fed back to a piezo

actuator in the green beam path. The final locking loop required is for the phase of the local oscillator used for homodyne detection. Depending on the quadrature to be measured, two different locking methods were implemented in the system. When the amplitude quadrature was to be measured continuously the error signal was obtained by monitoring the subtracted photocurrent from the two homodyne detectors, and mixing down at 15 MHz. In order to display the phase quadrature noise continuously we used the dc value of the subtracted photocurrents directly as our error signal. Regardless of the method, the error signal was used to control a piezo actuator in the local oscillator beam.

4 Classical gain

As a tool for optimising the mode-matching of the green beam into the OPA cavity we have systematically investigated the classical gain factor of the infra-red seed beam injected into the back port of the OPA [39]. If the green pump is turned off, the throughput for the non-impedance matched seed beam is given by: $\langle A_{out}^{no\ pump} \rangle = 2\sqrt{\gamma_c \gamma_b} \langle A_{in} \rangle / \gamma$. The seed beam is subjected to either amplification or de-amplification, depending on the chosen relative phase between the pump beam and the seed beam. The theoretical OPA gain can be found from the classical counterpart of equation (1) by taking the expectation values, setting the derivative to zero and solving for the (classical) subharmonic field. The general solution is rather complex since it includes a term in third order of the circulating subharmonic field. However, when the seed beam is de-amplified this cubic term, which reflects the depletion of the pump, can be ignored. The de-amplification factor then reduces to

$$g_{deamp} = \frac{\langle A_{out} \rangle^2}{\langle A_{out}^{no\ pump} \rangle^2} = \left(1 + \frac{\langle B_{in} \rangle}{\langle B_{th} \rangle} \right)^{-2} \quad (3)$$

where $\langle B_{th} \rangle$ is the pump amplitude at threshold for the corresponding OPO. At threshold we have $g_{deamp} = 1/4$, a result which is independent of the cavity parameters and the magnitude of the seed beam. The experimentally observed de-amplification is plotted in Figure 2 together with the theoretically predicted curve. The difference is due to the fact that the phase-matching temperature was optimised for maximum pump power. Consequently, some phase mismatch occurred at lower pump powers. When the pump and seed beam are in phase the gain of the device is inverted and the seed beam is now amplified. In this regime the cubic term mentioned above cannot be neglected. A theoretical plot of the degree of amplification is shown in Figure 2 together with experimental data. The maximum gain at threshold is given by the expression: $g_{amp}^{max} = (4\gamma\gamma_c)^{2/3}(\langle B_{th} \rangle / \langle A_{in} \rangle)^{4/3}$. From this formula we see that the maximum gain depends on the power of the seed beam, $\langle A_{in} \rangle$. In the measurement shown in Figure 2 an amplification factor of 106 ± 12 was obtained, but by using a seed beam of extremely low power gain factors of up to $10,000$ have been observed in this apparatus [29].
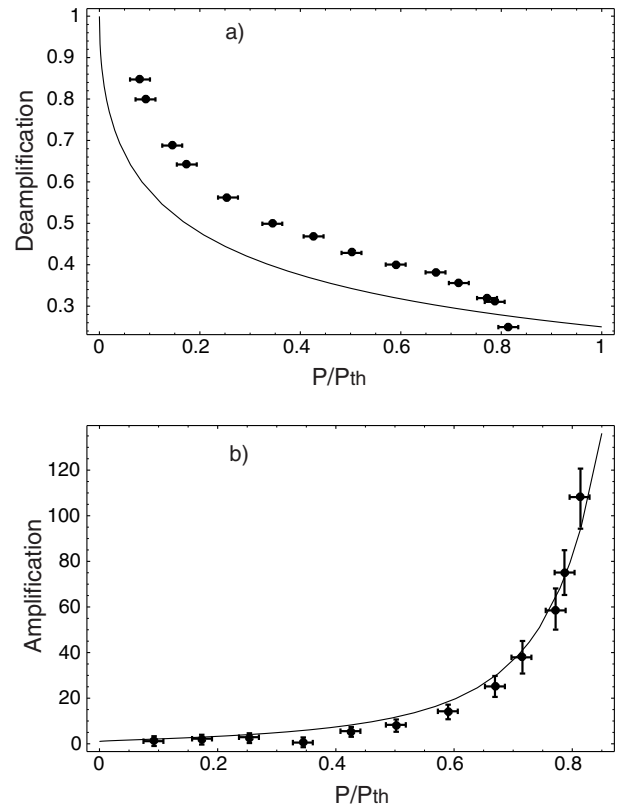

Fig. 2. Classical amplitude of the output of the parametric amplifier. (a) De-amplification of the input seed and (b) amplification of the input seed.

5 Squeezing

Our system can be operated in four different modes, all of which can be reached by changing the green pump phase and/or the power of the seed beam. The squeezing obtained in the four operation regimes will be denoted vacuum squeezing, bright amplitude squeezing, dim amplitude squeezing and bright phase squeezing, describing the intensity of the beam and the quadrature squeezed. The first three have been observed by several groups [23]. The latter type was generated by Breitenbach *et al.* [32] in the special case where the sideband under observation had a coherent amplitude, and by Zhang *et al.* [33] using the superposition of the two eigenmodes in a injection seeded nondegenerate OPA. However, to the best of our knowledge, so far there has been no demonstration of the production of single-mode phase squeezing where the optical field has a coherent excitation at the optical frequency.

5.1 Vacuum squeezing

When the injected coherent seed beam is removed and therefore replaced by the vacuum reservoir state, the degenerate down conversion produces spontaneous parametric fluorescence into the subharmonic mode of the optical parametric oscillator. In this case the intra-cavity subharmonic field is very low and the third order term in equation (1) can be neglected. Since the vacuum field does

not have a coherent excitation the operator A_{in} has zero mean. The spectral variance of the squeezed quadrature can easily be found

$$V^-(\Omega) = 1 - 4\eta \frac{\gamma_c}{\gamma} \frac{\langle B_{\text{in}}\rangle/\langle B_{\text{th}}\rangle}{(1 + \langle B_{\text{in}}\rangle/\langle B_{\text{th}}\rangle)^2 + (\Omega/\gamma)^2}. \quad (4)$$

Here the fraction γ_c/γ is the escape efficiency of the cavity and η indicates other losses which will lead to a reduction in the degree of observed squeezing as is a general consequence of the fluctuation-dissipation theorem. It includes the homodyne and detector efficiencies and losses in the beam path. A thorough discussion on limits to squeezing in the system can be found in reference [29]. It is obvious from equation (4) that the best squeezing is achieved when the pump power reaches the threshold value for the OPO. Although maximum squeezing is obtained near threshold the squeezing performance is not reduced considerably when decreasing the pump power to a value much lower than the threshold value. For example, pumping with 75% of the threshold value the maximum achievable squeezing would be limited to 98% (17 dB) assuming no losses.

The squeezed vacuum field produced by the OPA is subsequently detected by the homodyne system. By scanning the local oscillator phase, all projections of the whole quantum state becomes accessible. Figure 3a shows the phase dependence of the spectral variance of our squeezed vacuum beam at a fixed frequency of 3 MHz. The dips below the quantum noise limit represents the squeezing and as much as 5 dB of noise suppression below the quantum noise limit was observed.

5.2 Dim amplitude squeezing

Although the spontaneous parametric OPO produces very efficient squeezing it is difficult to obtain stable operation due to difficulties in locking the OPO cavity frequency to the frequency of the squeezed beam, which does not carry any coherent excitation. However, very stable operation can be achieved by injecting a coherent seed beam into the OPA and using the reflected part to lock the OPA cavity to the infra-red laser frequency. In order to avoid the transfer of technical noise from this beam to the squeezed beam, the seed beam carries very little power. We obtained a squeezed beam with a power of only about 1 μW and homodyne detection is required.

Using this method we obtained 5 dB of very stable squeezing for hours of operation but as much as 5.5 dB has been observed for smaller time periods. The noise suppression at a single frequency obtained for 1 hour of operation is shown in Figure 3b. Since the subtraction of the photocurrents in the homodyne system is efficient over a wide spectrum and the detectors used had a broadband electronic gain, we were able to record squeezing spectra from 2 MHz to 20 MHz. An example of such a measurement is shown in Figure 4a.
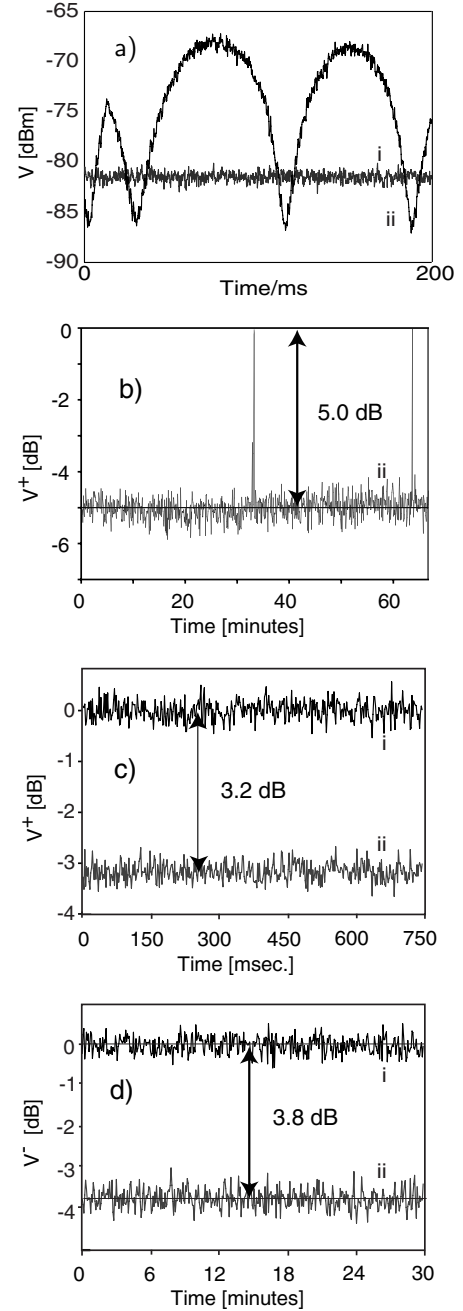

Fig. 3. Spectral densities for the fluctuations from the homodyne detection system shown in Figure 1. Traces (i) are the quantum noise limits and traces (ii) are the squeezing for four different types of operation. (a) Vacuum squeezing, (b) dim amplitude squeezing, (c) bright amplitude squeezing and (d) phase squeezing.

5.3 Bright amplitude squeezing

We do not need a local oscillator to measure amplitude squeezing if the optical power of the squeezed beam is bright enough to be detected directly. To reach this goal of direct detection we applied a very powerful seed beam and generated a squeezed beam with a power of 100 μW, which was directly detected. Unfortunately by doing this
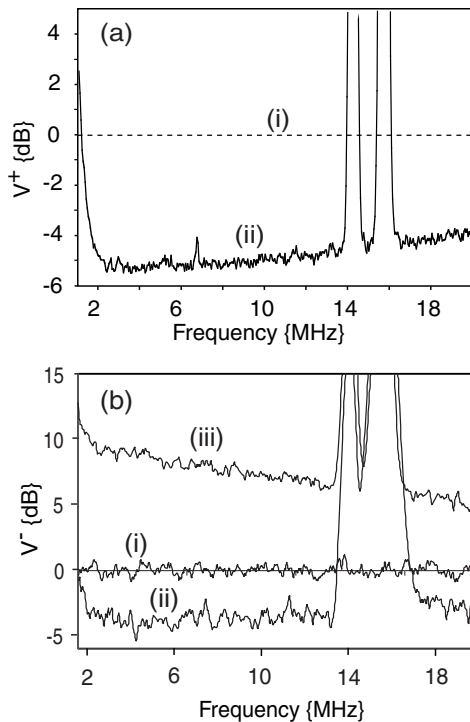
Fig. 4. Spectral density of the squeezed quadratures, for amplitude quadrature squeezing (a) and phase quadrature squeezing (b), as a function of detection frequency. Shown are the QNL (i), the actual noise in the squeezed quadrature (ii) and the anti-squeezed fluctuations (iii).

Fig. 5. Theoretical estimates of phase quadrature squeezing in an OPA as a function of the injected seed power for three different pump powers: 99% (dotted), 80% (dashed) and 10% (full line) of threshold power. The parameters used are those given in Section 3, $\mu = 0.015$ and $V_p^- = 1$.

we suffered a large reduction in the green pump power and we only observed around 3.2 dB of squeezing at 4.5 MHz as shown in Figure 3c. This type of squeezing could also be stabilized for long periods of times.

5.4 Phase squeezing

When the relative phase between the pump and the seed beam is rotated such that the OPA works as an amplifier, the amplitude quadrature noise is amplified while the phase quadrature noise is suppressed and therefore squeezed. To observe stable phase squeezing, the pump locking servo is now locked to maximum amplification of the seed beam, while the homodyne system is tuned to detect phase quadrature fluctuations. In the case of phase squeezing the intra-cavity field in the OPA cannot be neglected and hence the pump depletion term plays a role in the quantum process of amplification. The spectral variance is now given by

$$V^-(\Omega) = 1 - \eta \frac{8\gamma_c\sqrt{\mu}\langle B_{\text{in}}\rangle + 4\gamma_c\mu\langle a\rangle^2(1 - 2V_p^-)}{(\gamma + \mu\langle a\rangle^2 + 2\sqrt{\mu}\langle B_{\text{in}}\rangle)^2 + \Omega^2} \quad (5)$$

where V_p^- is the variance of the phase quadrature of the pump beam. Due to the importance of the pump depletion term, the phase quadrature squeezing behaves quite differently from the more common amplitude quadrature squeezing, where, as mentioned above, the pump depletion
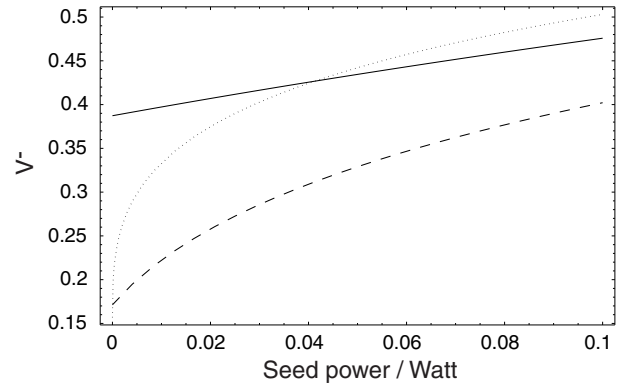
do not play a significant role. A theoretical plot showing the phase quadrature squeezing at 4.5 MHz as a function of the seed input power for various powers, P, of the pump beam is presented in Figure 5. Here we have assumed that the pump is quantum noise limited, in particular $V_p^- = 1$. The power is normalised to the threshold power P_{th} and the thick, dashed and dotted lines represent $P/P_{\text{th}} = 0.1$, $P/P_{\text{th}} = 0.8$ and $P/P_{\text{th}} = 0.99$, respectively. We see that maximum squeezing is not necessarily achieved near threshold, but at some pump power well below threshold. At zero seed power we see, as expected from the previous sections, that the squeezing improves as we approach the threshold. But an opposing impact of the injected seed beam on the phase squeezing is clearly seen from this figure. Just the slightest amount of seed power leads to a drastic reduction in the squeezing near threshold and lower pump powers becomes increasingly advantageous. For example, a seed power larger than 40 mW pumping with 10% of threshold value is better than using 99%. We conclude that the pump depletion term alters the squeezing properties of an OPA and phase quadrature squeezing behaves quite differently from amplitude quadrature squeezing.

By careful optimisation of the pump power for a given seed power, the OPA temperature and the electronic locking loops we achieved 4.2 dB of phase quadrature squeezing. Very low seed powers were employed, both because of the reason mentioned above but also because of requirement of the homodyne detection system, that the power of the squeezed beam has to be much lower than that of the local oscillator. After amplification we had around 20 μW of power in the squeezed beam and the local oscillator power was 2 mW. We demonstrate the long-term stability of the device, by recording the degree of noise suppression continuously for 1 hour. The average squeezing was 3.8 dB below the quantum noise level as shown in Figure 3d. Broadband phase quadrature squeezing is also demonstrated from 2 MHz to 20 MHz. This measurement is shown in Figure 4b. All the results presented here have been corrected for the dark noise of our detection
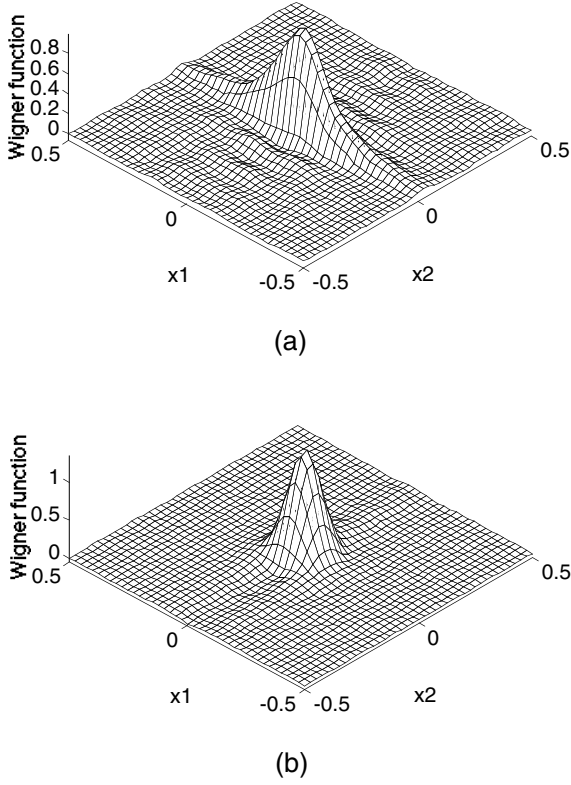
(a)

(b)

Fig. 6. Reconstructed Wigner functions for (a) a squeezed vacuum state and (b) an ordinary vacuum state.

system. We have not, however, corrected for the quantum efficiency of our detectors, which was found to be ∼93%.

6 An alternative detection technique: two-dimensional correlation plots

The results given above, and almost all other data reported for squeezed light, are based on using a homodyne detection system that measures the variance of the squeezed state *via* the difference of the photocurrents of the two detectors. The variance is determined in the frequency domain *via* an electronic spectrum analyser. This is a single quadrature measurement of a single quantum input. A demonstrated alternative is optical homodyne tomography (OHT) [32,41]. This is also based on a homodyne detection system, but the local oscillator is scanned to allow full reconstruction of the Wigner function of the input quantum state. The photocurrents from the detectors are not sent to a spectrum analyser, instead the currents are recorded by a high speed data acquisition system. This allows full reconstruction of the statistical moments of the data, albeit at some cost in terms of equipment and computing power. We have experimentally reconstructed the Wigner function associated with the squeezed vacuum state, generated by our OPA system. The OHT detection system is described in details in reference [42]. In Figure 6 we show the reconstructed Wigner function of a squeezed vacuum state (Fig. 6a) and of an ordinary vacuum state

(Fig. 6b). Using the latter state for calibration we find a squeezing degree of 4.1 dB. An important observation is the Gaussian nature of the Wigner functions, which is justifying the Gaussian claim made in the theoretical section.

An alternative technique, which is also based on homodyne detection, will now be described. The scheme is shown in Figure 1. Consider a homodyne system where a squeezed signal beam, s, is mixed with a strong local oscillator beam, β, at a 50/50 beam splitter, in order to create a pair of spatially separable quantum correlated beams. Each beam is detected and the generated photocurrents are demodulated independently at the RF detection frequency Ω_d. The demodulated signal is then low pass filtered with bandwidth $\delta\Omega$ to give a detection frequency of $\Omega_d \pm \delta\Omega$. These two processed photocurrents may now be sent to the x/y inputs of a digital storage oscilloscope. The displayed result is then a scatter diagram of the instantaneous amplitude quadrature fluctuations of the two sample beams. This setup therefore provides a real-time view of the joint fluctuations in a $2\delta\Omega$-bandwidth and the collected data yield the joint probability distribution function.

By visualising the instantaneous fluctuations, correlation between the photocurrents due to the quantum nature of the signal beam may now be observed directly on the oscilloscope. It will be shown below that the data contain the θ-quadrature of the signal beam, δX_s^θ, (set by the phase of the local oscillator with respect to the signal beam) and the amplitude quadrature of the local oscillator, δX_β^+. Like OHT, this technique bypasses the spectrum analyser therefore giving all statistical moments of the quadratures recorded, however it does not allow reconstruction of the Wigner function since only one quadrature is recorded.

Besides visualizing quantum correlation this technique provides quantitative information about the variance of the amplitude quadratures of the two beams emanating from the beam splitter, the quadrature variance of the weak signal beam, the amplitude quadrature variance of the bright beam and, finally, the correlation coefficient and conditional variances between the two possibly entangled beams. All this information is gained in a single measurement of the joint distribution function.

6.1 A more detailed description and interpretation

The demodulated photocurrents collected by the two homodyne detectors are given by:

$$\delta n_1^\theta(\Omega_d \pm \delta\Omega, t) = \frac{1}{2}\beta\{\delta X_\beta^+(\Omega_d \pm \delta\Omega, t)$$
$$+ \delta X_s^+(\Omega_d \pm \delta\Omega, t)\cos\theta + \delta X_s^-(\Omega_d \pm \delta\Omega, t)\sin\theta\} \quad (6)$$

$$\delta n_2^\theta(\Omega_d \pm \delta\Omega, t) = \frac{1}{2}\beta\{\delta X_\beta^+(\Omega_d \pm \delta\Omega, t)$$
$$- \delta X_s^+(\Omega_d \pm \delta\Omega, t)\cos\theta - \delta X_s^-(\Omega_d \pm \delta\Omega, t)\sin\theta\} \quad (7)$$
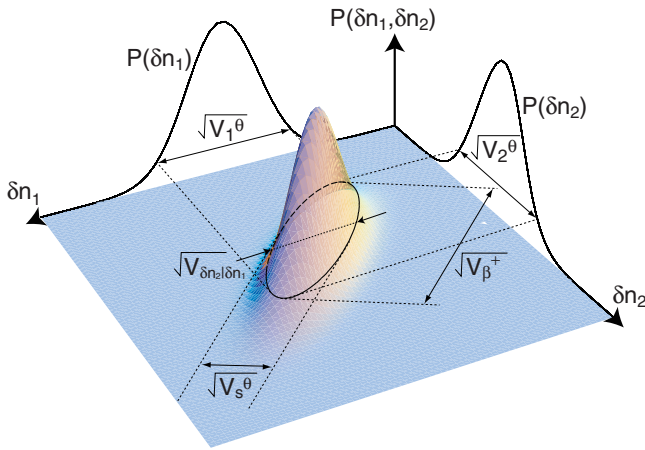
Fig. 7. Simulation of a joint density function, $P(\delta n_1, \delta n_2)$, for two partial correlated photocurrents, δn_1 and δn_2. The projected marginal density functions, $P(\delta n_1)$ and $P(\delta n_2)$, are also shown.

where δX_β^+ corresponds to the amplitude quadrature fluctuations of the local oscillator while δX_s^+ and δX_s^- are the amplitude and phase quadrature fluctuations of the input squeezed mode, respectively. β is the average, time independent coherent amplitude of the local oscillator and is assumed to be much greater than the coherent amplitude of the signal beam.

Successive measurements of these currents allow the construction of a two dimensional probability density distribution $P(\delta n_1^\theta, \delta n_2^\theta)$ of current amplitudes. As mentioned above, this is made visible by displaying the currents δn_1^θ and δn_2^θ simultaneously with an storage oscilloscope in x/y-mode. The density of dots, (as seen in the experimental results of Fig. 8) is proportional to the joint probability distribution function, $P(\delta n_1^\theta, \delta n_2^\theta)$, of the joint fluctuations. Since the fluctuations of the two photocurrents manifest individually Gaussian statistics, $P(\delta n_1^\theta)$ and $P(\delta n_2^\theta)$, the combined statistical realization, $P(\delta n_1^\theta, \delta n_2^\theta)$ is a bivariate Gaussian as shown in the simulation in Figure 7. A contour of the joint probability distribution will in general yield an ellipse.

The shape of $P(\delta n_1^\theta, \delta n_2^\theta)$ is determined by the correlation of the entangled pair, created by the squeezed beam and the beamsplitter. If the quadratures of the two beams are statistically independent the correlation between them is zero ($C^2 = 0$) and the two data sets create a circular, symmetric shape. Perfect correlation or anti-correlation ($C^2 = 1$) gives a straight line at either 45° or –45° with respect to the coordinate axis, while partial correlation (see Fig. 7) yields a shape of an ellipse oriented at ±45°. Other correlation angles are not possible since the system is perfectly balanced.

In addition to the two projected marginal distribution functions shown in Figure 7, projections on the +45° and −45° are also of high relevance as these marginal functions provide the probability distributions of the sum and difference currents of the two beams, respectively. In other words, the marginal distribution functions along the ±45°

axes give us a link back to conventional homodyne measurements. Therefore, the standard deviation along the +45° and the –45° axes correspond to the standard deviations of the sum and the difference of the photocurrents as would regularly be obtained from homodyne detection with a spectrum analyser. These, in turn, correspond to the standard deviations of the noise of the local oscillator, $\sqrt{V_\beta^+} = \sqrt{\langle |\delta X_\beta^+|^2 \rangle}$, and the signal beam, $\sqrt{V_s^\theta} = \sqrt{\langle |\delta X_s^\theta|^2 \rangle}$, as indicated in Figure 7. Finally, the conditional deviation, $\sqrt{V_{\delta n_2 | \delta n_1}}$, can be deduced by fixing one of the variables while considering the probability distribution of the other one, as shown in Figure 7.

The size of the scatter plot may be calibrated in the same way as any other homodyne measurements: by using the vacuum state. Setting the signal beam to be the vacuum state gives $\sqrt{V_s^\theta} = 1$, therefore providing a quantum noise reference for all other measurements. The existence of quantum entanglement and hence squeezing is thus visualised directly on the oscilloscope by the observance of a 45° tilted ellipse with a standard deviation less than that of the vacuum state.

The correlation coefficient, C, between the photocurrents may be found by measuring the standard deviations of the ±45° projections. Alternatively and more accurately, the coefficient can be calculated using all individual current data and the definition

$$C = \frac{1}{m\sqrt{V_1^\theta V_2^\theta}} \sum_{i=1}^{m} \left[\delta n_1^\theta \right]_i \left[\delta n_2^\theta \right]_i \qquad (8)$$

where m is the number of acquired pairs of data. This provides a value for C of high accuracy. This, in turn, may be used to find the variance of the signal beam V_s, as will be demonstrated below. In the simplest case, if the local oscillator is shot noise limited, we find $V_s = (1 - C)/(1 + C)$.

6.2 Using a quantum noise limited local oscillator

Examples of visualising the correlation created by mixing a phase squeezed beam and a quantum noise limited local oscillator at a beamsplitter are shown in Figure 8. Here the scatter plots of the joint density function are shown for different operating conditions with $m = 10,000$ pairs of acquired data at $\Omega_d/2\pi = 4.5$ MHz and a bandwidth of $\delta\Omega/2\pi = 100$kHz. The contours in Figure 8 are defined as the conditional deviation of the data as a function of the data angle (see Ref. [8b]). First we considered the case where the two beams are blocked and hence only the dark noise is recorded (Fig. 8a). Due to the nature of dark noise we expect the two measured variables to be statistically independent and hence the correlation to be vanishingly small. This is indeed the case and we measure a correlation of only $C^2 = 0.008$. Similarly, a small correlation is encountered when the squeezed beam is blocked, leaving only vacuum entering the homodyne system. This measurement is shown in Figure 8b and the correlation is measured to $C^2 = 0.009$. Unblocking the squeezed beam and setting
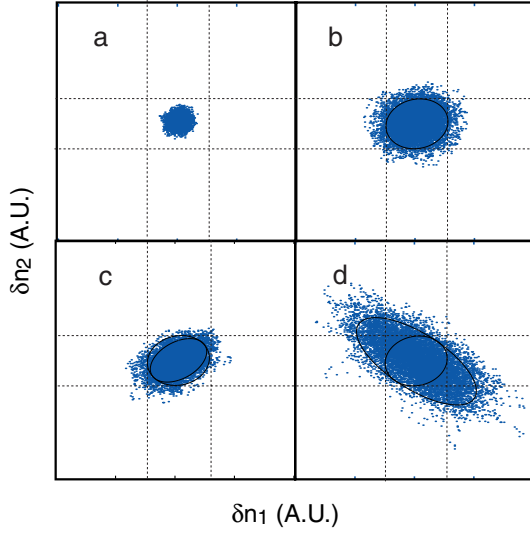
Fig. 8. Experimental two-dimensional correlation plots taken at 4.5 MHz. (a) All beams into the homodyne detection system are blocked and only the dark noise is recorded. (b) The local oscillator beam is unblocked while the other beamsplitter input port is illuminated by vacuum only. (c) Phase squeezing is created and the relative phase between the local oscillator and the squeezed beam is locked to $\theta = \pi/2$. (d) The relative phase is rotated to $\theta = 0$ in order to detect the correlations produces by the anti-squeezed quadrature.

the local oscillator phase to $\theta = \pi/2$ gives rise to quantum correlation between the two output beams from the beamsplitter. This is seen from equation (7) with $\theta = \pi/2$ and $\delta X_s^- \rightarrow 0$. The generated quantum correlation is clearly visualised in Figure 8c by an uncertainty area, which is squashed relative to the vacuum noise in Figure 8b. We measure a strong quantum correlation of $C^2 = 0.16$. Since the local oscillator is quantum noise limited the origin of the correlation is purely quantum mechanically. Setting the phase of the local oscillator relative to the squeezed beam to zero ($\theta = 0$) means that the noisy amplitude quadrature of the squeezed beam is detected and a strong anti-correlation between the two output beams is evident since the anti-squeezing is much bigger than the shot noise (see Eq. (8)). This anti-correlation is shown in Figure 8d with a correlation coefficient of $C^2 = 0.47$.

6.3 Using a local oscillator in a mixed state

The quantum noise limited nature of the local oscillator at 4.5 MHz was verified by the symmetry of the fluctuation circle in Figure 8b. However, at lower frequencies we expect that technical noise from the laser which passes through the mode-cleaner contributes classical noise to the local oscillator. This leads to a modification of the local oscillator noise in equation (7). The noise now consists of a quantum part, $\delta X_{\beta q}^+$, and a classical part, $\delta X_{\beta c}^+$, such that $\delta X_\beta^+ = \delta X_{\beta c}^+ + \delta X_{\beta q}^+$. For the two choices $\theta = 0$ and $\theta = \pi/2$ equations (7) now become (dropping the argu-
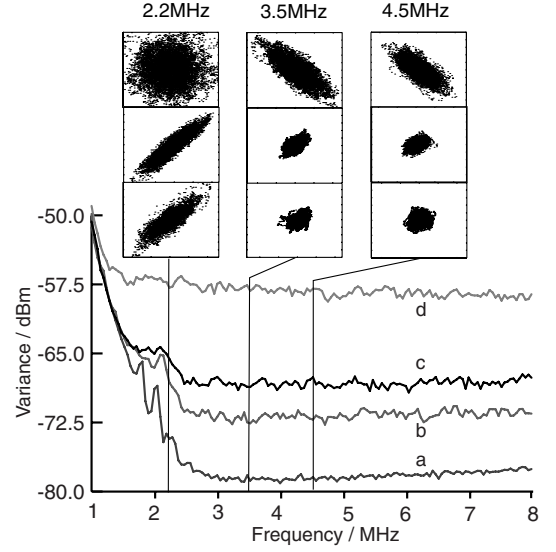

Fig. 9. Below: power spectrum of the (a) detectors dark noise, (b) the amplitude squeezing, (c) the shot noise and (d) the phase anti-squeezing. Above: two-dimensional correlation plots at three different frequencies and three different operation conditions; from the top $\theta = \pi/2$, $\theta = 0$ and with blocked signal beam.

ments for simplicity):

$$\delta n_{1,2}^0 \propto \frac{1}{2}\left(\delta X_{\beta q}^+ + \delta X_{\beta c}^+ \pm \delta X_s^+\right) \rightarrow \frac{1}{2}\left(\delta X_{\beta q}^+ + \delta X_{\beta c}^+\right)$$
$$\delta n_{1,2}^{\pi/2} \propto \frac{1}{2}\left(\delta X_{\beta q}^+ + \delta X_{\beta c}^+ \pm \delta X_s^-\right) \rightarrow \frac{1}{2}\left(\delta X_{\beta c}^+ \pm \delta X_s^-\right)$$

(9)

where we have used the fact that the fluctuations in the amplitude quadrature of the squeezed beam is small so $\delta X_{\beta q}^+ \gg \delta X_s^+$ and $\delta X_s^- \gg \delta X_{\beta q}^+$. Owing to the eventual classical excess noise in the local oscillator the correlation displayed by the scatter diagram may originate from quantum modulations in the squeezed beam as well as the classical modulations in the local oscillator beam. The total correlation we denote C_m, while the quantum correlation and the classical correlation is denoted by C_q and C_c, respectively. The three correlation coefficients are related through the expression:

$$C_q = \frac{(1 + V_e)(C_m - C_c)}{(1 + V_e)(1 - C_m)C_c + (1 - V_e)(1 - C_c)}$$

(10)

where V_e is the spectral variance of the electronic noise floor relative to the quantum noise level. The correlation of the electronic noise was found to be zero and therefore neglected in this expression.

Examples of mixed states are given in Figure 9, where the signal beam is amplitude quadrature squeezed and the local oscillator is either in a thermal state or in a coherent state depending on the detection frequency. The lower part of the figure shows the power spectrum of the electronic detector noise (a), the amplitude quadrature squeezing (b), the quantum shot noise (c) and the

amplitude quadrature anti-squeezing (d). At four distinct frequencies, 2.2 MHz, 3.5 MHz and 4.5 MHz, marked with vertical lines, we constructed the correlation plots shown in the upper part of the figure. Nine different plots were obtained; three at each frequency with $\theta = \pi/2$ (upper row), $\theta = 0$ (middle row) and when the amplitude squeezed beam is blocked such that only the amplitude quadrature of the local oscillator is monitored (lower row). In the latter case all quantum correlations are excluded and only correlations of pure classical origin are seen. At 4.5 MHz the classical correlation is negligible $C_c^2 = 0.01$ and can hardly be seen. Small visible classical correlations start to appear at 3.5 MHz ($C_c^2 = 0.08$), and at 2.2 MHz we see that they become very large with $C_c^2 = 0.67$. Turning our attention to the middle row pure quantum correlation at 4.5 MHz appears due to the squeezed beam and attains a value of $C_q^2 = 0.16$. At 3.5 MHz and at 2.2 MHz a mixture of quantum and classical correlation is seen with a total correlation of $C_m^2 = 0.37$ and $C_m^2 = 0.83$, respectively. Because we know the degree of classical correlation (lower row), the degree of total correlation (middle row) and the spectral variance of the dark noise, the pure quantum correlation can be inferred from equation (10). We calculate $C_q^2 = 0.18$, $C_q^2 = 0.22$ and $C_q^2 = 0.14$ at 2.2 MHz, 3.5 MHz and 4.5 MHz respectively. While equation (4) shows that the quantum correlation should be best at lower frequencies with maximum at zero, technical noise in the laser masks this effect. We see a trend from 4.5 MHz to 3.5 MHz with an enhancement of 0.08, but the correlation is reduced again at 2.2 MHz.

When the relative phase is switched to $\theta = \pi/2$ the phase quadrature anti-correlation originating from the squeezed beam is monitored together with the amplitude laser noise correlation as evident from equations (9). At 4.5 MHz and 3.5 MHz the anti-correlation dominates, with correlation of $C_m^2 = 0.51$ and $C_m^2 = 0.57$ respectively. However, at 2.2 MHz the laser noise becomes comparable to the anti-squeezing resulting in a big noisy uncorrelated state as is shown in the top left corner of Figure 9.

7 Conclusion

We have demonstrated four different modes of generating squeezed light using a monolithic degenerate optical parametric amplifier in the quantum regime. Efficient generation of vacuum squeezing, dim and bright amplitude quadrature squeezing and phase quadrature squeezing have been shown. We have demonstrated the reliability and stability of the squeezing and obtained 5 dB of amplitude squeezing over one hour of operation using five stable, electronic locking loops. In addition we have showed the first demonstration of bright phase squeezed light and achieved 4.2 dB noise suppression.

Quantum correlations as well as classical correlations were visualised directly by displaying the photocurrents of the two output beams that were created by mixing a squeezed beam with either a quantum noise limited or a thermal noisy local oscillator at a beamsplitter; a homodyne detection system. The degree of noise suppression

and the correlation coefficient for both the nonclassical signal beam and the local oscillator can be determined quantitatively. The results are very educational in that they are showing the different types of correlations directly and provide an attractive means of demonstrating the properties of squeezed light.

References

1. C. Fabre, Phys. Rep. **219**, 215 (1992), H.J. Kimble, Phys. Rep. **219**, 227 (1992)
2. K. McKenzie, D.A. Shaddock, D.E. McClelland, B.C. Buchler, P.K. Lam, Phys. Rev. Lett. **88**, 231102 (2002)
3. M. Xiao, L.A. Wu, H.J. Kimble, Phys. Rev. Lett. **59**, 278 (1987)
4. P. Grangier, R.E. Slusher, B. Yurke, A. La Porta, Phys. Rev. Lett. **59**, 2153 (1987)
5. E.S. Polzik, J. Carri, H.J. Kimble, Phys. Rev. Lett. **68** 3020 (1992)
6. Y.Q. Li, P. Lynam, M. Xiao, P.J. Edwards, Phys. Rev. Lett. **78**, 3105 (1997)
7. R. Bruckmeier, H. Hansen, S. Schiller, J. Mlynek, Phys. Rev. Lett. **79**, 43 (1997)
8. (a) B.C. Buchler, U.L. Andersen, P.K. Lam, H.-A. Bachor, T.C. Ralph, Phys. Rev. A **65**, 011803(R) (2002); (b) U.L. Andersen, B.C. Buchler, H.-A. Bachor, P.K. Lam, J. Opt. B **4**, S229 (2002)
9. A. Furusawa, J.L. Sørensen, S.L. Braunstein, C.A. Fuchs, H.J. Kimble, E.S. Polzik, Science **282**, 706 (1998)
10. T. Ralph, P.K. Lam, Phys. Rev. Lett. **81**, 5668 (1998)
11. S.L. Braunstein, H.J. Kimble, Phys. Rev. Lett. **80**, 869 (1998)
12. S. Lloyd, S.L. Braunstein, Phys. Rev. Lett. **82**, 1784 (1999)
13. S.D. Bartlett, B. Sanders, S.L. Braunstein, K. Nemoto, Phys. Rev. Lett. **88**, 097904 (2002)
14. S.L. Braunstein, H.J. Kimble, Phys. Rev. A **61**, 042302-1 (2000)
15. X. Li, Q. Pan, J. Jing, J. Zhang, C. Xie, K. Peng, Phys. Rev. Lett. **88**, 047904 (2002)
16. T.C. Ralph, Phys. Rev. A **61**, 010303 (2000)
17. M. Hillery, Phys. Rev. A **61**, 022309 (2000)
18. M.D. Reid, Phys. Rev. A **62**, 062308 (2000)
19. W.P. Bowen, R. Schnabel, H.-A. Bachor, P.K. Lam, Phys. Rev. Lett. **88**, 093601 (2002)
20. C. Fabre, J.B. Fouet, A. Maitre, Opt. Lett. **25**, 76 (2000)
21. N. Treps, U.L. Andersen, B. Buchler, P.K. Lam, A. Maitre, H.-A. Bachor, C. Fabre, Phys. Rev. Lett. **88**, 203601 (2002)
22. P.D. Drummond, K.J. McNeil, D.F. Walls, Opt. Acta **27**, 321 (1980); **28**, 211 (1981); G. Milburn, D.F. Walls, Opt. Commun. **39**, 401 (1981); C.W. Gardiner, M.J. Collett, Phys. Rev. A **31**, 3761 (1985); M.J. Collett, D.F. Walls, Phys. Rev. A **32**, 2887 (1985); M.J. Collett, R.B. Levien, Phys. Rev. A **43**, 5068 (1991)

23. H.-A. Bachor, *A guide to experiments in quantum optics* (Wiley, 1998)
24. H. Takahashi, *Adv. Commun. Syst. Theory Appl. 1* (Academic Press, New York, 1965), p. 227
25. A. Heidmann, R. Horowicz, S. Reynaud, E. Giacobino, C. Fabre, G. Camy, Phys. Rev. Lett. **59**, 2555 (1987)
26. Z.Y. Ou, S.F. Pereira, H.J. Kimble, K.C. Peng, Phys. Rev. Lett. **68**, 3663 (1992)
27. L.A. Wu, H.J. Kimble, J.L. Hall, H. Wu, Phys. Rev. Lett. **57**, 2520 (1986)
28. G. Breitenbach, T. Muller, S.F. Pereira, J.-Ph. Poizat, S. Schiller, J. Mlynek, J. Opt. Soc. Am. B **12**, 2304 (1995)
29. P.K. Lam, T.C. Ralph, B.C. Buchler, D.E. McClelland, H.-A. Bachor, J. Gao, J. Opt. B **1**, 469 (1999)
30. K. Schneider, R. Bruckmeier, H. Hansen, S. Schiller, J. Mlynek, Opt. Lett. **21**, 1396 (1996)
31. K. Schneider, M. Lang, J. Mlyenk, S. Schiller, Opt. Expr. **2**, 59 (1997)
32. G. Breitenbach, S. Schiller, J. Mlynek, Nature **387**, 471 (1997)
33. Y. Zhang, H. Wang, X. Li, J. Jing, C. Xie, K. Peng, Phys. Rev. A **62**, 023813 (2000)
34. C.W. Gardiner, P. Zoller, *Quantum Noise* (Springer, 1999)
35. R.W.P. Drever, J.L. Hall, F.V. Kowalski, J. Hough, G.M. Ford, A.J. Munley, H. Ward, Appl. Phys. B **31**, 97 (1983)
36. D. Shaddock, M.B. Gray, D.E. McClelland, Opt. Lett. **24**, 1499 (1999)
37. D.A. Shaddock, B.C. Buchler, W.P. Bowen, M.B. Gray, P.K. Lam, J. Opt. B **2**, 1 (2000)
38. Perfect squeezing is obtained theoretically using linearized theory. However, the linearisation approximation brakes down near threshold were the squeezing is largest. Using a full quantum model without linearization of the operators, Chaturvedi *et al.* [40] found that the squeezing scales with $N^{-3/2}$ where N is the photon number
39. G. Breithenbach, S. Schiller, Mod. Opt. **44**, 2207 (1997)
40. S. Chaturvedi, K. Bechoum, P.D. Drummond, Phys. Rev. A **65**, 033805 (2002)
41. D.T. Smithey, M. Beck, M.G. Raymer, A. Faridani, Phys. Rev. Lett. **70**, 1244 (1993)
42. J.W. Wu, P.K. Lam, M.B. Gray, H.-A. Bachor, Opt. Exp. **3**, 154 (1998)